Constraining axion-like particles using the white dwarf initial-final mass relation

JCAP 00 (2021) 010

Matthew J. Dolan, Frederick J. Hiskens, Raymond R. Volkas

ARC Centre of Excellence for Dark Matter Particle Physics, School of Physics, The University of Melbourne, Victoria 3010, Australia

Axion-like particles & the energy-loss argument

Axion-like particles (ALPs) are pseudoscalars which appear frequently in extensions of the Standard Model (SM) of particle physics. The eponymous example is the QCD axion[1-4] , but hundreds of ALPs can arise in manifold compactification scenarios in string theory[5].

ALPs which evade terrestrial detection could be produced within stellar interiors[6]. If sufficiently light and weakly interacting, they can freely escape the star, thereby providing a new source of stellar **energy-loss**. This affects stellar structure by reducing the local energy gain rate per unit mass ϵ.

The response of the stellar medium to additional energy-loss, as illustrated in Figure 1, results in the acceleration of nuclear burning phases. If this acceleration contradicts astronomical observation, then such an ALP can be excluded. This mechanism is termed the **energy-loss argument** and constraints derived in this manner are known as **stellar cooling** bounds.

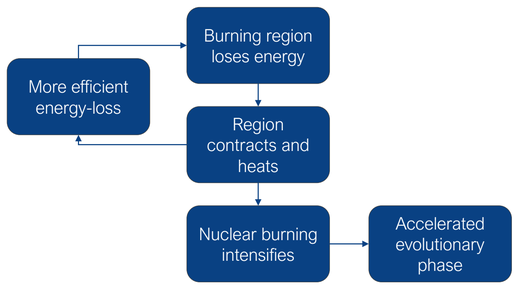

Figure 1: Illustration of the energy-loss argument, which serves as the basis of stellar cooling constraints.

Astrophysical ALP production

Throughout this work we restrict our attention to ALPs which couple solely to electromagnetism via the two-photon vertex

$$\mathcal{L}_\gamma = -\frac{g_{a\gamma\gamma}}{4} a F_{\mu\nu}\tilde{F}^{\mu\nu}.$$

Here $g_{a\gamma\gamma}$ is the ALP-diphoton coupling strength, a is the ALP field and F and $\tilde{F}$ are the electromagnetic field strength tensor and its dual.

These ALPs have two production mechanisms of importance in a stellar interior. These are the **Primakoff process** (Figure 2a), the conversion of a thermal photon into an ALP in the presence of an external electromagnetic field, and **photon fusion** (Figure 2b).

The energy-loss rate to ALPs per unit mass is given as a sum over these two processes and can be expressed as:

$$\epsilon_a = \frac{g_{a\gamma\gamma}^2 T^7}{4\pi\rho}(G_P(\xi,\mu) + G_F(\mu))$$

where T is the temperature and ρ is the local mass-density. The functions G_P and G_F involve integrals over photon phase space appropriate for the Primakoff process and photon fusion respectively. Both functions are sensitive to the temperature-normalized ALP mass $\mu = m_a/T$ and are Boltzmann suppressed when $\mu \gtrsim 1$. G_P additionally depends on the temperature normalized Debye-Hückel wavenumber $\xi = k_s/2T$, which sets the screening scale for the Primkaoff process.

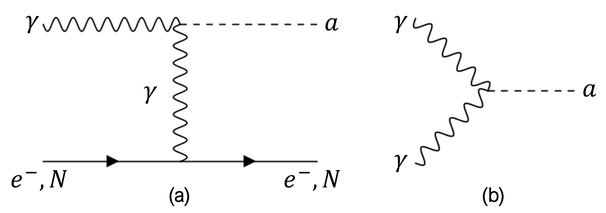

Figure 2: Feynman diagrams for ALP production via the Primakoff process **(a)** and photon fusion **(b)**.

Exploring the parameter space

The most restrictive stellar cooling constraints on m_a-$g_{a\gamma\gamma}$ parameter space comes from limits on the lifetime of **horizontal branch (HB)** stars[7], the central helium burning phase of low mass stars ($\lesssim 2M_\odot$). The keV-MeV mass range of this constraint is shown in yellow in Figure 3. Such stars have core temperatures of roughly 8.6 keV, which causes the constraint to relax in the shown mass range.

Other relevant constraints in this region come from the visible[8] (blue) and neutrino[9] (red) signals of SN1987A and the SLAC E137 electron beam dump experiment[10]. These fail to constrain a small triangular region at $m_a \sim 1\ MeV$ and $g_{a\gamma\gamma} \sim 10^{-5}\ GeV^{-1}$. While big bang nucleosynthesis excludes this region, this can relax in viable non-standard cosmological scenarios. It has therefore come to be known as the **cosmological triangle**.

The purpose of this work is to use arguments from stellar evolution to further constrain the cosmological triangle. To do this one must consider evolutionary phases which have higher characteristic temperatures than HB cores. We chose to target ALP effects on the subsequent (hotter) shell helium burning phase – the **asymptotic giant branch**.

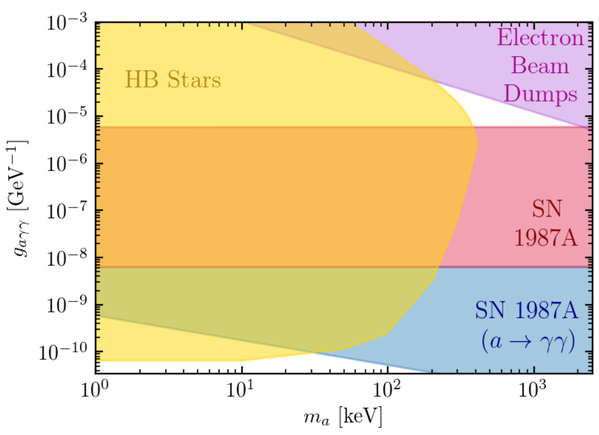

Figure 3: The keV-MeV mass range of m_a-$g_{a\gamma\gamma}$ parameter space. The constraints shown come from the lifetime of horizontal branch stars[7], the visible[8] and neutrino[9] signals of SN1987A and the SLAC E137 electron beam dump experiment[10].

Asymptotic giant branch stars

The asymptotic giant branch (AGB) is the evolutionary phase immediately following central helium burning in stars with initial masses between $0.6\text{-}8M_\odot$. They have cores composed of carbon/oxygen, surrounded by a **helium-rich layer**, at the base of which is a **helium-burning (He-B) shell**.

Encasing these is a **hydrogen-rich layer** which supports a **hydrogen-burning (H-B) shell** at its base. This also hosts a deep **convective envelope** which extends from the stellar surface and efficiently mixes its contents. The AGB is separated into two phases: the early (E)-AGB and the thermal pulsating (TP)-AGB.

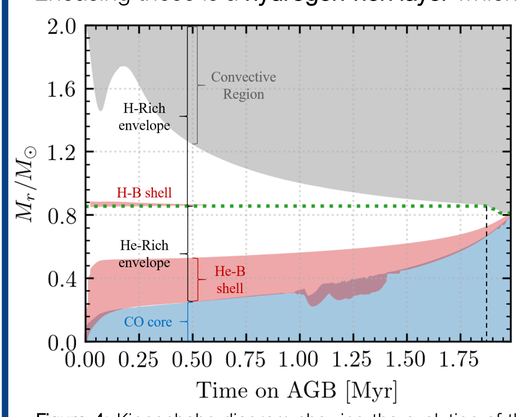

Figure 4: Kippenhahn diagram showing the evolution of the CO core (blue), He-B and H-B shells (red) and convective envelope (grey) in terms of the radial mass coordinate M_r (i.e. the mass interior to a spherical shell of radius r). The extent of these regions after 0.5 Myr on the AGB is labelled. Included in dotted green is the H/He discontinuity (the boundary between H-rich and He-rich layers).

The E-AGB evolution of a $4M_\odot$ star is shown in Figure 4 (consult the caption for a description). The evolution of this phase is governed by the activity of the He-B shell, which progresses outward through the He-rich layer, causing the CO core to grow. Simultaneously, nuclear burning activity therein increases, which favors the expansion of the outer layers and allows the convective envelope to penetrate more deeply within the star.

In stars more massive than $4M_\odot$ the convective envelope can extend into the helium-rich layer. The helium therein is dispersed throughout the outer envelope, curtailing the growth of the CO core. This event is termed the **second dredge-up**.

During the subsequent TP-AGB strong stellar winds strip way the star's outer layers exposing the degenerate CO core, which goes on to form the bulk of the white dwarf.

ALPs & the second dredge up

It is known that ALPs can increase the efficiency of the second dredge-up and decrease the CO core mass M_{CO}[11]. However, the sensitivity of M_{CO} to ALPs has never been assessed in the keV-MeV mass range. We investigate this by simulating the evolution of the E-AGB with and without energy-loss to ALPs using the 1D stellar evolution code *Modules for Experiments in Stellar Astrophysics* (MESA)[12-16].

Figure 5 displays the E-AGB evolution of $4M_\odot$ stars with (centre, right) and without (left) novel energy-loss to ALPs. The model shown in the central panel includes 10 keV ALPs with $g_{a\gamma\gamma} = 0.66 \times 10^{-10}\ \mathrm{GeV}^{-1}$, at the boundary of the HB constraint. The right panel depicts a model with 316 keV ALPs with $g_{a\gamma\gamma} = 10^{-9}\ \mathrm{GeV}^{-1}$, within the Boltzmann suppressed region. The CO core mass at the end of the E-AGB is labelled.

In both scenarios M_{CO} is reduced in the presence of ALPs. The same is not true for the E-AGB duration which does not decrease substantially in the Boltzmann suppressed case.

Our simulations indicate that more massive stars, which have hotter He-B shells, are more sensitive to ALPs in the Boltzmann suppressed region. For example, in a $6M_\odot$ star, M_{CO} of a $6M_\odot$ star decreased from $0.96M_\odot$ to $0.81M_\odot$ when the same ALP parameters as in the right panel of Figure 6 were adopted.

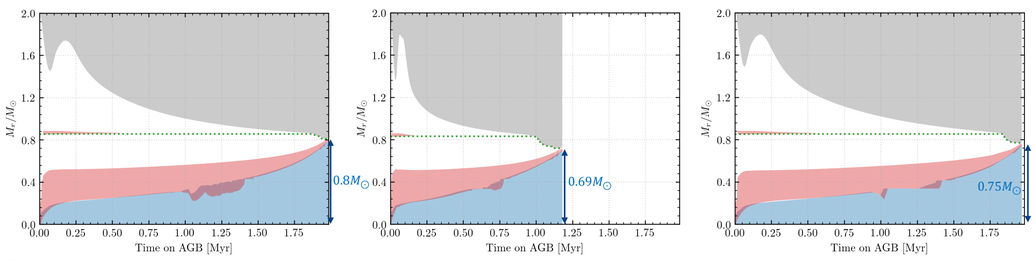

Figure 5: Kippenhahn diagrams showing the E-AGB evolution of $4M_\odot$ stars with (centre, right) and without (left) energy-loss to ALPs. The simulation shown in the central panel was conducted with 10 keV ALPs with $g_{a\gamma\gamma} = 0.66 \times 10^{-10}\ \mathrm{GeV}^{-1}$, while that of the right panel used 316 keV ALPs with $g_{a\gamma\gamma} = 10^{-9}\ \mathrm{GeV}^{-1}$.

The white dwarf initial-final mass relation

The initial-final mass relation (IFMR) relates the mass with which a star forms on the Main Sequence to that of the white dwarf into which it ultimately evolves. It is typically modelled as a three-piece linear function with breakpoints at $2\text{-}2.8M_\odot$ and $3.6 - 4M_\odot$.

As the TP-AGB is relatively short in stars more massive than about $4M_\odot$, little structural change occurs to the CO core during this phase. The impact of ALPs on M_{CO} shown in the previous panel is therefore maintained in the final white dwarf mass, enabling the IFMR to be used to limit this behavior

Numerous constraints on the IFMR exist. However, we chose to utilize one derived from the observation of 14 wide double white dwarf binaries[17], as it eliminated unwanted sensitivity to star cluster age-determination. This makes it less restrictive than others, so its selection is a conservative choice. Favored IFMRs are indicated by the green region in Figure 6.

Note that this constraint is semi-empirical, as it uses progenitor lifetime functions and white dwarf cooling times derived from theoretical models. The addition of ALPs to stellar models reduces the magnitude of the former, and therefore affects the derivation of the binary constraint. However, it can be shown that taking account of this would shift the green region in Figure 6 upwards, while ALPs drag theoretical IFMRs downwards. This effect can therefore be neglected.

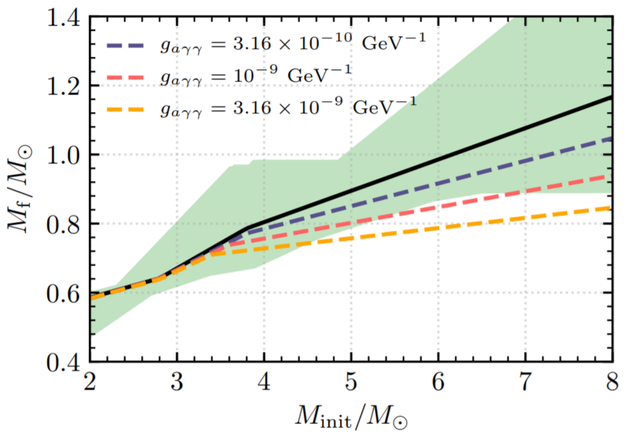

Figure 6: Plot showing theoretical IFMRs generated without ALPs (black) and with 316 keV ALPs given the couplings shown in the top-left. The allowed region according to [17] is shown in green.

ALPs & the IFMR

We investigated the effects of ALPs on the IFMR in the following manner:

1. Simulate the evolution of stars with initial masses between $2\text{-}8M_\odot$ in $0.2M_\odot$ intervals from before the Main Sequence until the end of the TP-AGB **without** ALPs and record their final masses.
2. Apply a three-piece linear fit with flexible breakpoints to these data. This is indicated by the black line in Figure 6.
3. Repeat, but include ALPs given a specific choice of m_a and $g_{a\gamma\gamma}$.

Example IFMRs are shown in Figure 6 given energy-loss to 316 keV ALPs with coupling strengths as indicated in the Figure. Of these, only the yellow IFMR can be excluded.

A constraint has been derived by repeating this procedure while scanning over ALP mass. The smallest excluded value of $g_{a\gamma\gamma}$ for each value of m_a was noted. These collectively define the dark blue line in Figure 7. This does not extend to arbitrarily high couplings, as they cause ALPs to decay within the He-B shell, invalidating the energy-loss argument.

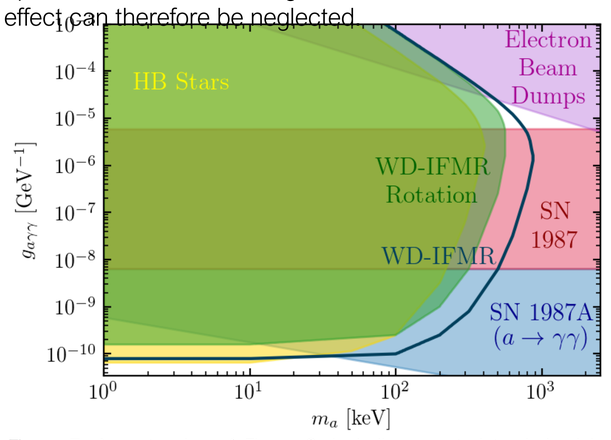

Figure 7: An extension of Figure 3, including constraints derived in this work without (dark blue line) and with (green) accounting for stellar rotation.

This constraint had to be modified to account for systematic uncertainty concerning the modelling of the IFMR. The most important source of this was **stellar rotation**, which shifts theoretical IFMRs upward by an average of between $0.04\text{-}0.08M_\odot$ depending on the strength of rotational mixing in the model[18]. We accounted for this by shifting all theoretical IFMRs generated upwards by $0.08M_\odot$ and re-deriving our constraint. The final constraint is shown in green in Figure 7.

Rotation also extends progenitor lifetimes which should cause the green region in Figure 6 to shift downwards. However, as the estimated magnitude of this effect was considerably smaller than $0.08M_\odot$, we have neglected this possibility.

Future prospects

Theoretical and observed properties of evolving stars have long been a powerful tool for investigating physics beyond the Standard Model. In this work we demonstrated the sensitivity of M_{CO} to axion-like particles and constrained this behavior using the white dwarf initial-final mass relation. Several conservative choices resulted in our constraint being substantially outperformed by horizontal branch stars at low ALP masses. Despite this, we were able to further constrain the cosmological triangle. Our constraint stands to improve dramatically as theoretical and observational uncertainties are better understood. For example, 1400 new double white dwarf binaries have been catalogued in the recent Gaia early data release 3[19]. If even 10% of these are wide, it could see the sample size of our adopted IFMR constraint improve tenfold.

References

[1] R. Peccei et al., *Phys. Rev. Lett.* **38** (1977) 1440
[2] R. Peccei et al., *Phys. Rev. D* **16** (1977) 1791
[3] S. Weinberg, *Phys. Rev. Lett.* **40** (1978) 223
[4] F. Wilczek, *Phys. Rev. Lett.* **40** (1978) 279
[5] A. Arvanitaki et al., *Phys. Rev. D* **81** (2010) 123530
[6] G. Raffelt, *University of Chicago Press* (1996)
[7] P. Carenza et al., *Phys. Lett. B* **809** (2020) 135709
[8] J. Jaeckel et al., *Phys. Rev. D* **98** (2018) 055032
[9] G. Lucente et al., *JCAP* **12** (2020) 008
[10] J. Bjorken et al., *Phys. Rev. D* **38** (1988) 3375
[11] I. Dominguez et al., *MNRAS* **306** (1999) L1
[12] B. Paxton et al., *ApJS* **192** (2011) 3
[13] B. Paxton et al., *ApJS* **208** (2013) 4
[14] B. Paxton et al., *ApJS* **220** (2015) 15
[15] B. Paxton et al., *ApJS* **234** (2018) 34
[16] B. Paxton et al., *ApJS* **243** (2019) 10
[17] J. Andrews et al., *ApJ* **815** (2013) 63
[18] J. Cummings et al., *ApJ* **871** (2019) L18
[19] K. El-Badry et al., *MNRAS* **506** (2021) 2269

This research was supported in part by the Australian Research Council and the Australian Government Research Training Program Scholarship Initiative